Combustion and Flame 183 (2017) 30–38

Contents lists available at ScienceDirect

Combustion and Flame

journal homepage: www.elsevier.com/locate/combustflame

Measurement of reaction rate constants using RCM: A case study of decomposition of dimethyl carbonate to dimethyl ether

Peng Zhang[a,1], Shuang Li[b,1], Yingdi Wang[c], Weiqi Ji[a], Wenyu Sun[a], Bin Yang[a,*], Xin He[c], Zhi Wang[c], Chung K. Law[a,d], Feng Zhang[b,*]

[a] Center for Combustion Energy and Department of Thermal Engineering, Tsinghua University, Beijing 100084, PR China
[b] National Synchrotron Radiation Laboratory, University of Science and Technology of China, Hefei 230029, PR China
[c] State Key Laboratory of Automotive Safety and Energy, Tsinghua University, Beijing 100084, PR China
[d] Department of Mechanical and Aerospace Engineering, Princeton University, Princeton, NJ 08544, USA

ARTICLE INFO

Article history:
Received 21 February 2017
Revised 26 March 2017
Accepted 5 May 2017
Available online 18 May 2017

Keywords:
Rate constant measurement
Rapid compression machine
Fast sampling
Methyl formate
Dimethyl carbonate

ABSTRACT

This paper proposes a method to measure the reaction rate constants in kinetically-simple pyrolysis systems using rapid compression machine (RCM) and fast sampling. The method involves first performing sensitivity analysis based on a reasonable kinetic model to identify the species dominated by a target reaction. Then the time-resolved species concentration profiles are measured in RCM experiments using fast sampling and gas chromatography. Finally, the pre-assigned pre-exponential factor and the activation energy are optimized by an iterative fitting procedure, in which the entire temperature profile derived from the pressure history is taken into account. In order to validate this method, the rate constant of the reaction CH_3OCHO (methyl formate, MF) => CH_3OH+CO (R1) was determined by measuring the CO concentration over 948–1112 K at 30 bar, obtaining the rate expression $k_{R1}/s^{-1} = 3.04 \times 10^{13} \exp(-30968\ K/T)$, which is consistent with previous theoretical and experimental studies. The rate constant of the reaction $CH_3OCOOCH_3$ (dimethyl carbonate, DMC) => CH_3OCH_3 (dimethyl ether, DME)+CO_2 (R2) was then studied by measuring the time-resolved DME concentration over 994–1068 K at 30 bar. The measured rate expression of $k_{R2}/s^{-1} = 2.02 \times 10^{13} \exp(-34248\ K/T)$ with an uncertainty of ±30% agrees well with the RRKM/Master Equation calculation based on a high-level quantum chemical potential energy surface.

1. Introduction

Assignment of rate constants for important combustion reactions is a crucial aspect in the development of detailed combustion chemical kinetic models for hydrocarbon fuels and biofuels. Among various well developed experimental methods to measure the rate constants [1], shock tube (ST) combined with laser absorption spectrometry (LAS) has been widely used in the study of pyrolytic reaction under high-pressure and high-temperature conditions [2–3]. A key assumption of this method is that if the uncertainty of the concentration of an individual species is predominantly influenced by a single reaction in a complex reaction system, the rate constant of this reaction can be derived from the measured concentration time-history of that species. For instance, Ren et al. [4–5] studied the decomposition of methyl formate (MF) using ST combined with LAS over 1202–1607 K and 1.36–1.72 atm. The CO, CH_2O, and CH_4 concentrations are dominated by the reactions MF => CH_3OH+CO, MF => $2CH_2O$, and MF => CH_4+CO_2, respectively. The rate constants of these reactions were then obtained by tuning them to match the measured mole fractions of CO, CH_2O, and CH_4. Over the last decade, this method has contributed extensively to the development of combustion kinetic models of typical hydrocarbons and biofuels [2–3]. Another successful application of shock tube on the rate constant measurement is the single-pulse shock tube (SPST) [6–7]. In these experiments, gas chromatography (GC) is used to analyze the sample withdrawn from the reactive mixture, which is quenched by the expansion wave after a specific reaction time (typically 0.5–2.0 ms). The rate constants are then derived from the concentration-temperature plots. With the temperature uncertainty significantly reduced by the comparative method of Tsang [8], SPST has been extensively used in the study of unimolecular decomposition and some bimolecular reactions [9].

In view of the success achieved by the technique of ST/LAS and SPST on the measurement of reaction rate constants, we apply herein the similar concept to the rapid compression machine

* Corresponding authors.
E-mail addresses: byang@tsinghua.edu.cn (B. Yang), feng2011@ustc.edu.cn (F. Zhang).
[1] Peng Zhang and Shuang Li contributed equally to this work.

http://dx.doi.org/10.1016/j.combustflame.2017.05.006
0010-2180/

(RCM) combined with fast sampling and GC. Compared to the traditional ST/LAS and SPST, RCM usually operates with a longer test time (~10 ms in this study), which means it can be used for the measurements of slower reactions at lower test temperatures. With a longer test time, RCM can be used as a supplementary tool to the ST measurements; while with a lower test temperature, more species will be dominated by a corresponding single reaction, which enables more applications of this method. Additionally, compared to ST/LAS, RCM/GC can be used to simultaneously quantify large molecules and multiple species without interference, which also extends the potential application of this method; while compared to SPST, RCM/GC has adjustable test times over multiple reproducible experiments, which will result in concentration-time plots instead concentration-temperature plots in SPST.

RCM, typically used for the study of homogenous combustion and ignition, has been proven effective and reliable in kinetic modeling studies [10]. In particular, the crevice piston design, which eliminates the corner vortex [11–12] scratched from the cold boundary layer by piston motion and thereby tremendously extends the duration of the homogenous hot core, was first proposed by Lee and Hochgreb [13] in 1998 and subsequently adopted by almost all RCMs. The success of this design was confirmed by computational fluid dynamics (CFD) calculations [14–17] and non-intrusive temperature measurements [15,18], leading to the consensus that, with this design, the homogeneity in the bulk mixture can be easily maintained longer than 20 ms after the end-of-compression (EOC). This homogeneity also supports the adiabatic core assumption, making it possible to derive the temperature by the adiabatic relation, which has also been validated by laser diagnostics [19–21].

There are two non-ideal aspects in the RCM experiment compared to the ST experiment, namely the non-negligible compression process and the heat loss. Bradley et al. [22] has shown that these facility-dependent effects are the main reasons for the deviation of experimental data from different groups. The most commonly used correction method is that of “effective volume” [10,18,23], which assumes the entire process in the RCM core gas is adiabatic, and supplements the traditional constant volume simulation with a volume profile. The pressure increase/decrease due to the compression/heat loss is exactly replicated by shrinking/expanding the reactor volume before/after the EOC, hence providing a way to compare the experimental data with model predictions. This correction, together with the crevice piston design, has dramatically improved the reliability of the RCM data, rendering the RCM an important facility in the study of low- to intermediate-temperature combustion kinetics [10].

In addition to the ignition delay times of combustible mixtures, efforts have also been made to measure species concentrations using ex-situ speciation technique combined with GC. Some studies [18,24–27] were conducted by quenching the entire reaction chamber. However, the boundary layer and the piston crevice could complicate interpretation of the results [10,28]. An alternative method is to use the “fast sampling system” [29], in which a sampling probe is inserted into the middle of the combustion chamber to extract a sample from the hot core region, thereby minimizing the effects of the cold gas from the boundary layer and the crevice. For instance, thirty intermediate species were identified and quantified by He et al. [29] for iso-octane ignition. The concentrations of most species showed good consistency with previous model predictions [30]. More applications of this technique were subsequently reported for combustion studies of n-heptane [31], n-butanol [32], n-heptane/n-butanol blends [33], and methyl-butanoate [34]. While previous studies were conducted under relatively low pressures (3–10 bar) [29,31–34], recently Ji et al. [35] developed a fast sampling system with much higher operating pressure (~25 bar), which was used to study iso-butanol ignition.

Considering the species diagnostic capabilities of RCM mentioned above, we shall therefore explore the possibility of measuring rate constants using the RCM combined with a fast sampling system. In the following sections, the proposed experimental facilities and methodology are introduced first. Then as a validation of this method, the rate constant of methyl formate (MF, CH_3OCHO) decomposing to methanol and CO,

$$CH_3OCHO => CH_3OH + CO \quad (R1)$$

is measured and proved consistent with previous experimental [4] and theoretical [36–37] studies. Subsequently, the rate constant of

$$CH_3OCOOCH_3 => CH_3OCH_3 + CO_2 \quad (R2)$$

which is one of the most important decomposition channel in the pyrolysis of dimethyl carbonate (DMC, $CH_3OCOOCH_3$) [38–39], is measured and compared with our high level theoretical calculations.

2. Methodology

2.1. Rapid compression machine and fast sampling system

Experiments were conducted in a well-characterized RCM [40]. It is a pneumatically driven and hydraulically decelerated RCM with a crevice piston, a fixed stroke of 500 mm and a large bore of 50.8 mm. A mixture of fuel and argon is compressed to high pressure and high temperature within 25–30 ms. Then the pressure and temperature in the reaction chamber are slightly reduced due to heat loss after the EOC. The pressure history is measured using a piezoelectric pressure transducer (KISTLER 6125C) mounted on the reaction chamber. The same RCM has been used to study the ignition of n-heptane [40], iso-octane [40–41], and iso-butanol [35], with good consistency with literature results. Details of the RCM are given in these papers.

The fast sampling system, previously developed to withdraw stable species from the reaction chamber [35], was modified in the present study to minimize the sample loss during the sampling process. As shown in Fig. 1, the system mainly consists of a sampling probe, a fast-acting sampling valve, a sampling tank, the first transfer line to the sample inlet of the GC, the second transfer line from the sample outlet of the GC, and a vacuum pump. All the wetting areas, including the transfer lines, the sampling tank, and the sampling valve, are heated up to 393 K and evacuated before the sampling experiment. Noting that the extracted sample was stored in the sampling tank and then transferred to the GC by a syringe in the previous study [35], the sampling tank was directly connected to the inlet of the GC in the present study. Consequently, the high-pressure, high-temperature mixture in the reaction chamber expands to the sampling system as well as the sample loop of the GC simultaneously during the period (2.5 ms) when the solenoid valve is kept open. The equilibrium pressure in the sampling system is recorded by a pressure sensor (KISTLER 4045A) mounted on the sampling tank. It represents the sample amount and is used to normalize the peak area in the analysis of the GC results. Typically, the sample amount is less than 0.4% of the mixture in the reaction chamber, resulting in an equilibrium pressure of 0.3 bar in the sampling system. A commercial GC (Agilent 7890B) was used for species detection and quantification (GC conditions and sample chromatograms are provided in the Supplemental Material). Only one sample was withdrawn from the reaction chamber in a single shot. A series of experiments were conducted to sample

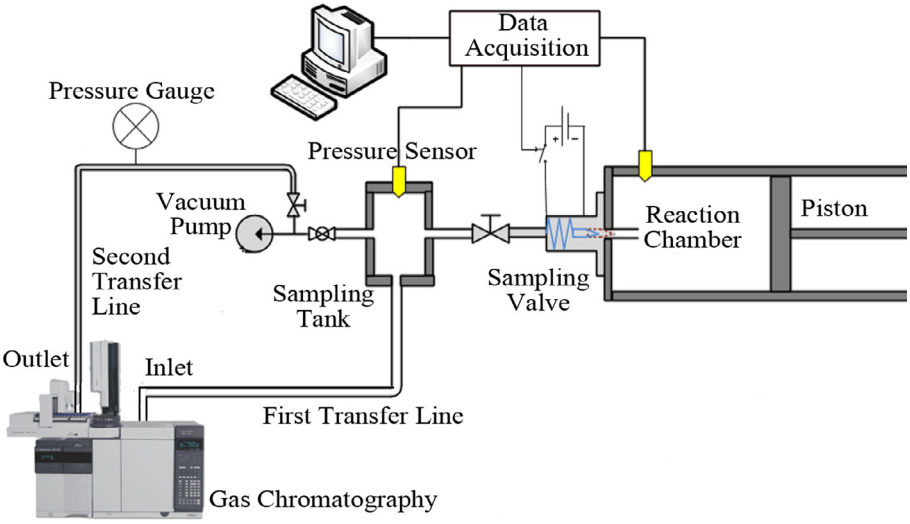

Fig. 1. Schematic of the fast sampling system.

at different times after the EOC, yielding a time-resolved species concentration profile. The dilution effect of the dead volume in the probe was corrected according to [35].

The concentration profiles of CO and DME were measured respectively in the MF and DMC experiments to derive the rate constants. Furthermore, in the MF experiments CO_2, CH_4, MF, and CH_3OH were also quantified to check the balance of the carbon and oxygen atoms. The calibrations of CO, DME, CO_2, and CH_4 were conducted using standard gases, while home-made MF/Ar mixtures were used to calibrate the MF mole fractions. Effective carbon number method was used to estimate the mole fractions of CH_3OH. The uncertainty in the sampling and quantification process will be discussed in Section 3.1. The sampling time window is 2.5 ms, which is determined from the pressure profile of the sampling tank.

2.2. Test mixtures and test conditions

All the test mixtures were prepared manometrically in a 20 L stainless-steel mixing tank. The mass of the fuels injected into the mixing tank was measured using a balance with 0.1 mg accuracy as a double check. The MF experiments were conducted at room temperature for its high vapor pressure. For DMC, experiments with fuel concentration higher than 0.5% were conducted with the mixing tank, the transfer line, and the reaction chamber heated to 356 K with a heating jacket to avoid potential condensation. The deviation of the temperature on the axis of the reaction chamber is within 1.5 K of the setting temperature. The temperatures of the mixing tank and the transfer line are maintained 5.0 K below the setting temperature to avoid condensation or overheat. The operation pressure for the sampling experiment is in the range of 25–45 bar for the present facility, recognizing that lower pressure will result in insufficient sample while higher pressure will lead to leakage of the sampling valve. Increasing the diameter of the probe and the orifice of the sampling valve would correspondingly increase the amount of the sample obtained, which could extend the operation pressure range of the current facility.

Mixture compositions and test conditions are shown in Table 1. The experimental temperatures selected herein are based on the analysis of the recently published MF [36–37] and DMC [38] models so that the CO concentration in the MF experiments and the DME concentration in the DMC experiments are dominated by R1 and R2 respectively. This is accomplished by sensitivity analysis shown later in Section 3. The lowest temperatures are 940 K for the MF experiments, and 980 K for the DMC experiments, which are limited by the detection limit of the present GC analysis system. Consequently the initial mole fractions of MF and DMC are increased with decreasing experimental temperature; with the MF experiments conducted under 30 bar, 948–1112 K, 0.05–3.99% MF in Ar, and the DMC experiments conducted under 30 bar, 980–1080 K, 0.38–2.71% DMC in Ar.

Table 1
Mixture compositions and test conditions.

No.	Fuel name	Percent (%)		p_{eff} (bar)	T_{eff} (K)
		Fuel	Ar		
1	MF	0.05	99.95	28.56	1112
2	MF	0.24	99.76	29.14	1099
3	MF	0.50	99.50	28.90	1075
4	MF	1.01	98.99	27.88	1043
5	MF	1.50	98.50	27.48	1009
6	MF	2.01	97.99	26.70	980
7	MF	3.99	96.01	30.10	948
8	DMC	0.38	99.62	28.87	1068
9	DMC	1.96	98.04	30.00	1060
10	DMC	2.11	97.89	30.27	1046
11	DMC	2.23	97.77	29.77	1033
12	DMC	2.36	97.64	29.93	1023
13	DMC	2.50	97.50	29.90	1011
14	DMC	2.71	97.29	29.85	994

2.3. Temperature profile in the RCM

Figure 2 shows a typical temperature profile in the RCM, deduced from the adiabatic relation:

$$\int_{T_0}^{T_t} \frac{\gamma}{\gamma - 1} d\ln T = \ln\left(\frac{p_t}{p_0}\right) \quad (1)$$

where T_0, p_0, p_t, and γ are the initial temperature, the initial pressure, the pressure history, and the specific heat ratio, respectively. Similar to previous studies [35,40–41], a slight pressure oscillation is observed around the EOC; a typical pressure profile is provided in the Supplemental Material. Consequently, time-zero (0 ms) is defined as the first peak in the pressure history around the EOC; the sharp temperature rise before time-zero is induced by the compression. The temperature at time-zero is denoted as T_C. The slight temperature rise after time-zero is due to a slight movement of the piston, resulting in a maximum temperature, T_{max}. The subsequent steady decrease is due to the heat loss. Typical

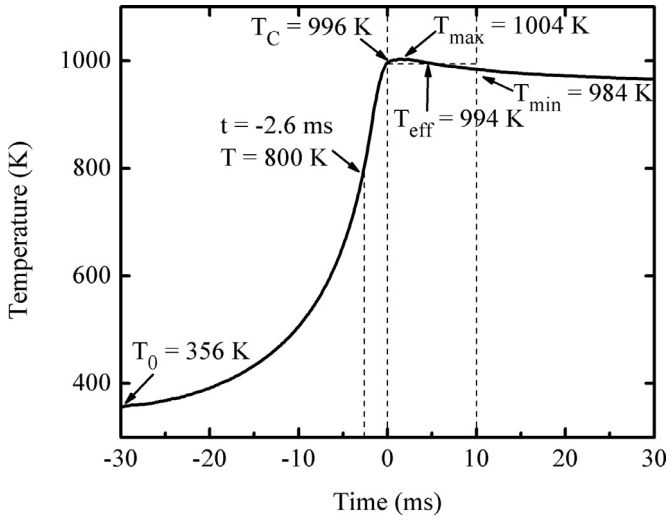

Fig. 2. Representative temperature profile in the RCM.

test time of the RCM experiment for ignition is 5–100 ms [10]. However, longer test times will expose the mixture to a broader temperature range, which means the results are more likely to be disturbed by non-zero-dimensional factors such as heat transfer. Both the adiabatic assumption and the kinetically dominant relation can be maintained at a slightly longer test time (*e.g.* 20 ms), and can be affected at a much longer test time (*e.g.* 100 ms). However, discussion of the test time limit is beyond the scope of this paper. The test time in the present work was selected to be 10 ms; that is most of the reported CO and DME mole fractions were collected during the period of 0–10 ms. The temperature at 10 ms is denoted as T_{min}. It is nevertheless also noted that preliminary tests up to 20 ms were performed, yielding results that are consistent with those of the 10 ms cases.

Figure 2 shows that the temperature in the RCM experiment varies with time, instead of being constant in the ST experiment. It rises dramatically during the compression and drops slightly after the EOC. This behavior does not affect the feasibility of the rate constant measurement because the temperature can be characterized by Eq. (1) and considered in the batch reactor model by varying the volume [23]. Effective pressure (p_{eff}) and effective temperature (T_{eff}) are used in the present study to report the corresponding conditions of the measured rate constants. The effective pressure is defined as the integral average of the pressure during 0–10 ms. The effective temperature is the temperature corresponding to the effective pressure. According to our tests, regardless of which temperature, T_C, T_{max}, T_{eff}, or T_{min}, is used to denote the experiment condition, the fitted Arrhenius expression will converge to a similar expression.

2.4. Rate constant optimization method

The rate constant is optimized by the following steps:

(1) Optimize the Arrhenius *A*-factor to best fit the simulation results to the measured CO (or DME) concentration profile, which yields an optimized rate constant for a specific effective temperature. A series of rate constants for different effective temperatures are thus obtained.
(2) Fit the optimized rate constants for a series of effective temperatures to the Arrhenius expression $k = A \times \exp(-E/T)$, and obtain an optimal *A*-factor, A_{opt}, and an optimal activation energy, E_{opt}.
(3) Take the fitted Arrhenius expression $k = A_{opt} \times \exp(-E_{opt}/T)$ as the new rate expression. Repeat the above procedure until the activation energy and the measured rate constants converge. The converged A_{opt} and E_{opt} are reported as the measured rate expression.

The best-fit in step (1) is defined by,

$$Q(f) = \sum_{i=1}^{n} \left(F^{t_i}_{spc,\ cal}(f) - \chi^{t_i}_{spc,exp}\right)^2 \quad (2)$$

where *Q(f)* is the target function to be minimized, *n* the number of experiments under this condition, $\chi^{t_i}_{spc,exp}$ the measured CO (or DME) mole fraction at the time t_i, and $F^{t_i}_{spc,\ cal}(f)$ the function that describes the relation between the factor *f* and the predicted CO (or DME) mole fraction at t_i. The function $F^{t_i}_{spc,\ cal}(f)$ is fitted from a series of simulations conducted by varying the factor *f* in the range of 0.1–10. The residual of $(F^{t_i}_{spc,\ cal}(f) - \chi^{t_i}_{spc,exp})$ represents the deviation of the simulation from the experiment at t_i, and *Q(f)* represents the total deviation of the simulation from the measured concentration profile under this condition.

Simulations presented herein were performed in a batch reactor with the program Cantera [42]. The facility effects, including the compression and the heat loss processes, were considered by specifying a dimensionless volume profile to the batch reactor. The volume profiles, which were derived from adiabatic relation using initial temperatures, initial pressures, and pressure profiles measured in the experiments, were normalized to the volume at the EOC. All the volume profiles used in this paper are provided in the Supplemental Material. Dooley's model [36] and Felsmann's model [37] were used in the study of reaction R1. It is noted that in Dooley's model [36], which has been widely tested and proven effective to predict species concentrations in shock tube, flow reactor, and flame experiments, the activation energy of R1 was obtained by analogy while the A-factor was adjusted to fit their flow reactor experiment. On the other hand, the more recently developed Felsmann's model [37] is based on the Sandia-Argonne's MF model [43–46] and contains Klippenstein's calculation for R1, which has not been formally published yet. These two models, however, predict almost identical results in this study. Consequently, only the predictions based on Felsmann's model will be presented to avoid cluttering of the figures.

A recently reported model for DMC combustion by Sun et al. [38] was used to study reaction R2. It has been tested against various experiments including flow reactor experiment, shock tube ignition delay, and laminar flame speed.

2.5. Rate constant calculations for DMC decomposition

As suggested in previous studies [38–39], the first two lowest energy channels, *i.e.* $CH_3OCOOCH_3 \Rightarrow CH_3OCH_3 + CO_2$ and $CH_3OCOOCH_3 \Rightarrow CH_3OC(O)O + CH_3$ strongly dominate DMC decomposition. Thus, in order to validate the accuracy of our rate constant measurement for R2, these two channels were investigated by high level quantum chemical calculations and RRKM/Master Equation (ME) simulations. The quadratic configuration interaction calculation including single and double substitutions (QCISD) [47] with the cc-pVTZ basis set [48] was used to optimize the related stationary points and compute the vibrational frequencies. Single point energies were corrected at the level of CCSD(T)-F12 [49] with the optimized correlation consistent basis set, VTZ-F12 [50]. The barrierless C–O bond fission were stepwise optimized with the step size of 0.1 Å at the level of B3LYP/cc-pVTZ [51], while the dissociation energy was scaled at the level of CCSD(T)-F12/VTZ-F12. The optimization and Hessian analysis were performed by the Gaussian09 program package [52] while the CCSD(T)-F12 energies were computed with the MOLPRO 2012 program [53]. The RRKM/ME calculations with a microcanonical vari-

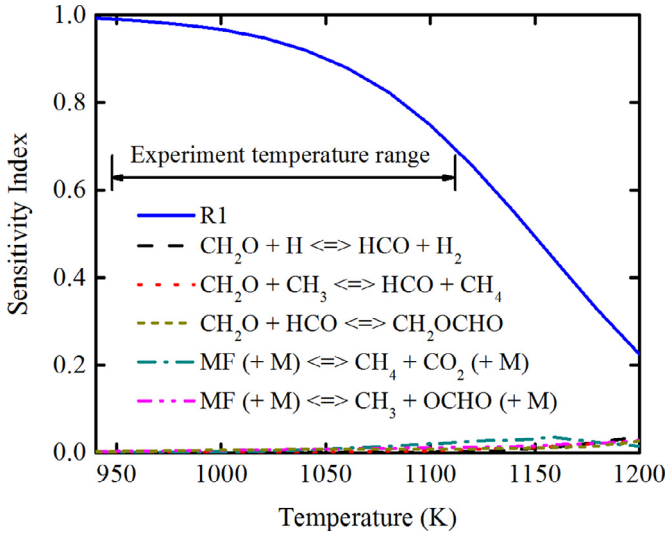

Fig. 3. Sensitivity analysis result of CO production in the pyrolysis of MF at 30 bar and 940–1200 K using Felsmann's model [37]. Solid line is the sensitivity of reaction R1.

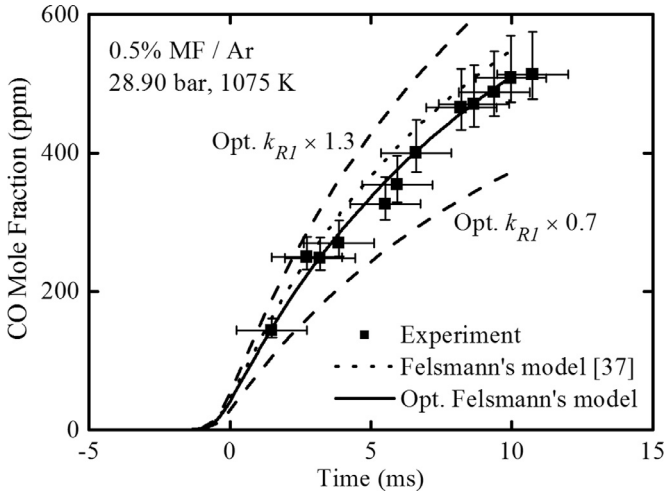

Fig. 4. Typical measured time histories of CO mole fraction (square) in the MF experiments. Dotted line is the CO mole fractions predicted by the original Felsmann's model [37]. Solid line is the CO mole fractions predicted by the optimized Felsmann's model. The variation of opt. $k_{R1} \pm 30\%$ (dashed lines) shows the uncertainty of the measured rate constant.

ational treatment for the barrierless C–O bond fission were performed within the temperature range of 700–1800 K at 0.5, 1, 10, 30, 100 atm, with the kinetic code – MESS [54–55]. The torsional modes corresponding to the internal rotation of -CH_3 were treated as 1-D hindered rotors, while the hindrance potential was computed at the level of B3LYP/cc-pVTZ. The asymmetric Eckart tunneling assumption [56] was used to estimate quantum tunneling effects. The collisional energy transfer function was represented by a single-parameter exponential down model with $<\Delta E>_{down} = 200 \times (T/298)^{0.85}$ cm^{-1}, which was also adopted by Sun et al. [38–39]. Lennard–Jones parameters were empirically estimated [57], for Ar, $\sigma = 3.47$ Å, $\varepsilon = 114$ K and for DMC $\sigma = 5.53$ Å, $\varepsilon = 440$ K.

3. Results and discussion

3.1. Validation experiment: MF => $CH_3OH + CO$

In this section, the rate constant of R1 was measured and compared with those from previous experimental [4] and theoretical [37] studies to validate the proposed method. Sensitivity analysis was performed first to identify the suitable experimental temperature range, in which the production of CO is dominated by reaction R1. The sensitivity index S_i is defined by,

$$S_i = \frac{\chi_{CO,\,i} - \chi_{CO,\,0}}{\chi_{CO,\,0}} \times \frac{1}{0.25} \quad (3)$$

where $\chi_{CO,\,0}$ is the original predicted CO concentration at 10 ms, where the subscript i is the reaction index, and $\chi_{CO,\,i}$ is the predicted mole fraction of CO when the A-factor of reaction i is increased by a factor of 0.25. Therefore, the physical meaning of the sensitivity index defined in Eq. (3) is the percentage increase in the CO production.

Figure 3 shows the top six sensitive reactions in the temperature range of 940–1200 K calculated with the Felsmann's model [37]. The production of CO is dominated by R1 in this range. However, the dominance of R1 is gradually reduced with increasing initial temperature. Meanwhile the secondary reactions become more important. Consequently, the MF experiments were conducted below 1120 K.

Figure 4 shows a representative time-resolved CO profile (squares) measured in the MF experiments for mixture No.3, together with the simulation results calculated with the original Felsmann's model [37] (dotted line) and the updated Felsmann's model (solid and dashed lines). Only one sample was extracted in one shot. Consequently, twelve experimental samplings at different times were conducted under the same condition to obtain the CO profile shown in Fig. 4. The measured CO mole fraction profile is quite smooth and the data scatter is small, implying that the repeatability of the facility is reasonable. The predicted production of CO begins before time-zero, which is the time of the EOC, then closely follows the measured results, indicating the compression process and the heat loss have been adequately considered in the variable volume batch reactor model. The prediction of the original Felsmann's model is located within the uncertainty of the measured results. The ± 30% variation of optimized k_{R1} in Fig. 4 shows the uncertainty of the derived rate constants, which will be discussed at the end of this section. Examples of measured profiles for other detected species are shown in the Supplemental Material.

Similarly, experiments were conducted for mixtures No. 1–7, obtaining seven time-resolved CO profiles for seven effective temperatures ranging between 948 and 1112 K. The rate constants were optimized using the methodology descripted in Section 2.4. Specifically, the rate constants in the Felsmann's model were used as a starting guess, which has an activation energy of 62.86 kcal/mol. For each effective temperature, the pre-exponential A-factor was tuned to best fit the simulation results with the measured CO profile, yielding a corresponding reaction rate for the effective temperature. In total, seven rates were obtained for seven effective temperatures. They are fitted to the Arrhenius expression, achieving a new activation energy of 61.36 kcal/mol. This process was repeated and converged after two iterations. The converged k_{R1} are shown in Fig. 5. The converged Arrhenius expression is $k_{R1}/s^{-1} = 3.04 \times 10^{13} \exp(-30968\ K/T)$, which is validated at 30 bar over the temperature range of 948–1112 K.

Figure 5 also shows the comparison of the measured k_{R1} with a previous ST measurement [4] and the prediction of Felsmann's model [37]. Felsmann's model predicts strong pressure dependence of R1 over the ST experimental temperature range (1202–1607 K) and weak pressure dependence in the RCM experimental temperature range of 948–1112 K. At 1.5 bar, the model agrees with the ST experiments with 12% root mean square (RMS) error. At 30 bar, it agrees with the present RCM experiments with 15% RMS error.

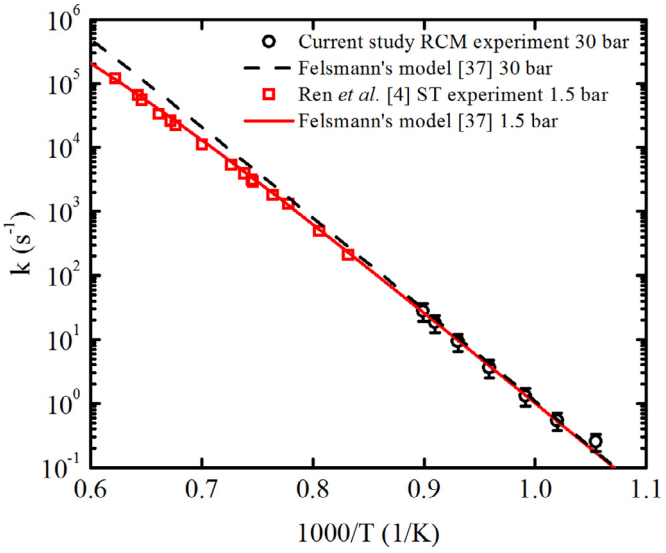

Fig. 5. Comparison of the measured k_{R1} with previous experimental [4] and theoretical [37] rates of reaction R1. Circles: RCM experiments at 30 bar from this study; squares: ST experiments at 1.5 bar from Ren et al. [4]; dashed line: Felsmann's model [37] at 30 bar; solid line: Felsmann's model [37] at 1.5 bar.

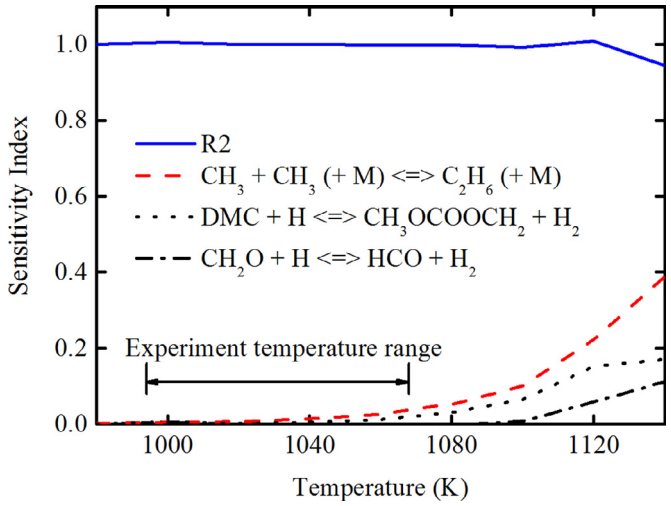

Fig. 6. Sensitivity index of DME production in the pyrolysis of DMC under 30 bar and 980–1140 K, obtained by using Sun's model [38]. Solid line is the sensitivity of reaction R2.

In the above experiments, MF and other main products, *i.e.* CH_4, CO_2, and CH_3OH, were also measured and quantified (shown in the Supplemental Material, Table S2) to check the carbon and oxygen atoms balance. 93–96% of the total carbon and oxygen atoms were recovered in the quantified species, which is considered to be satisfactory for speciation studies [35]. The primary reason for the carbon and oxygen loss is the potential condensation of MF in the sampling probe [35]. Moreover, the carbon and oxygen atoms in the unquantified unimportant species could make up 1% of the total amount according to the model.

In this study, the uncertainty of the measured rate constant is mainly introduced by the mixture temperature determination, the sampling and quantification process, the fitting error, and secondary reaction effects. The mixture temperature is determined by the adiabatic core assumption, which has been proven reasonable and well accepted in non-sampling studies [14–18]. Based on the consistency observed in Fig. 5, it is reasonable to conclude that the assumption also holds well with a sampling probe inserted in the reaction chamber, as otherwise the measured rates would be significantly lower than the literature results. Consequently, according to the adiabatic assumption, the uncertainty of the mixture temperature mainly comes from the uncertainty of the initial temperature (±1.5 K) measured by the thermocouple, the initial pressure (±860 Pa) measured by the static pressure sensor, the pressure history (±0.4%) measured by the cylinder pressure transducer, and the mixture composition (less than ±0.1%) determined by the pressure sensor and electronic balance. They together result in an uncertainty of ±5.2 K in T_{eff} in a single shot. Additionally, a series of experiments typically has a standard deviation of ±2 K in the determined mixture temperature. Consequently, the uncertainty in T_{eff} is estimated to be ±5.6 K, which can be converted to an uncertainty of 25% in the measured rates.

The sampling and quantification process is another major source of the uncertainty. In every single experiment, only less than 0.4% gas is extracted from the reaction chamber. Therefore, the temperature in the reaction chamber is barely affected by the sampling process. Once the sampling probe opens, the gas instantaneously expands to the sampling system driven by the pressure difference of 3–6 orders of magnitude. The fast expansion cools the sample and quenches the reaction, preserving the stable species as it was in the reaction chamber; while the reactive radicals in the sample may end up as stable species. The main uncertainty sources introduced in this process are the dead volume dilution, the recombination of the radicals, and the wall loss. The uncertainty in the dead volume dilution is estimated to be 2–8% according to the previous study [35]. The uncertainties introduced by radical recombination are characterized to be less than ±5% by the Cantera simulation. The sampling valve is kept open for 2.5 ms, which means that the uncertainty in the sampling time is ±1.25 ms. Normalization of the sampling amount has an uncertainty of ±2%, considering the equilibrium pressure (0.3 bar) and the uncertainty of the pressure sensor (±0.005 bar). The uncertainty from the gas chromatography measurement is conservatively estimated to be within ±10%. In total, the sampling and quantification process has an uncertainty of ±15% in the species concentrations and the rate constants.

The fitting error is introduced into the rate when fitting the pre-exponential A-factor to match the measured concentration. It is estimated to be ±5% based on the RMS of the deviation. The uncertainty from the secondary reaction effect is estimated to be within ±5% by comparing with the results after tripling the rate constants of the top five sensitive secondary reactions.

According to the above analysis, the overall uncertainty in the measured rates is estimated to be ±30%. Based on the consistency shown in Fig. 5 and the uncertainty analysis, it is reasonable to conclude that the proposed method has merit, and as such is promising in further studies.

3.2. Rate constant measurement: DMC => DME + CO_2

In this section, the rate constant of R2 was studied as an application of the proposed method. Sensitivity analysis was performed first using Sun's model [38] according to Eq. (3) introduced in Section 3.1. As shown in Fig. 6, in the DMC pyrolysis system, the production of DME is primarily sensitive to R2 over the temperature range of 980–1140 K. With increasing temperature, secondary reactions become more important since they all consume the products of the competition reactions, such as CH_3 and CH_2O. Consequently, the DMC experiments were conducted below 1080 K. Additional sensitivity analysis performed by multiplying the pre-exponential A-factor by 1.5 and 2.0 resulted in similar conclusion. Note that while the other product of reaction R2 is CO_2, it is inap-

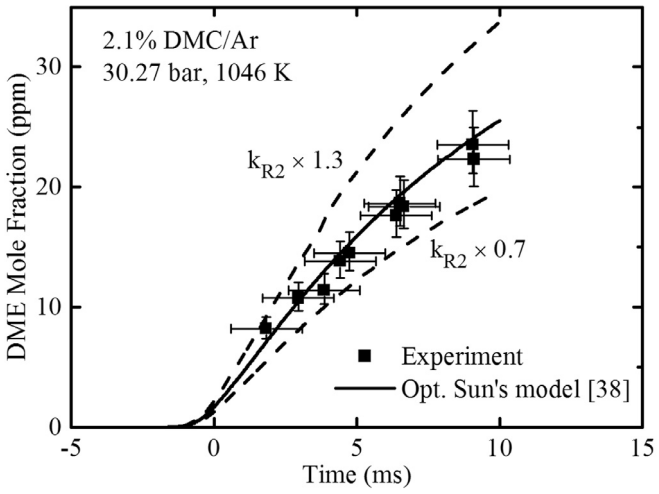

Fig. 7. Example of measured DME mole fraction time-histories (square). Solid line is the predicted DME mole fractions using Sun's model [38] with k_{R2} replaced by the optimized one. The variation of $k_{R2} \pm 30\%$ (dashed lines) shows the uncertainty of the optimized rate constant.

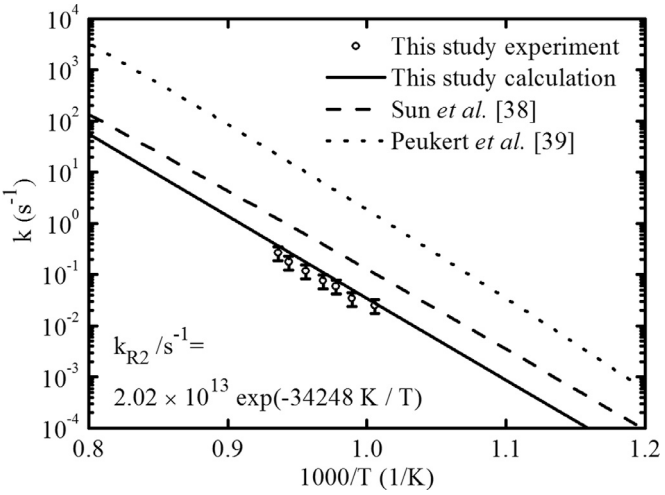

Fig. 8. Comparison of measured k_{R2} (square) with theoretical calculations. Dash-dot line: calculated k_{R2} from this study; dashed line: calculated k_{R2} from Sun et al. [38]; dotted line: calculated k_{R2} from Peukert et al. [39]. Pressure: 30 atm.

propriate to derive the rate constant by quantifying CO_2 because it is not dominated by R2.

Figure 7 shows a representative measured DME concentration profile (solid squares); ten experiments with different sampling times were performed with mixture No. 10, yielding the DME profile shown. The solid line is the prediction calculated using the updated k_{R2}. The dashed lines show the uncertainty range of the concentration prediction introduced by the uncertainty of k_{R2}. The measured DME concentrations and their error bars are covered by the uncertainty range of the concentration prediction. The original model over-predicts the DME concentration by a factor of 5 and as such its prediction is not shown. Examples of the measured profiles for other detected species are shown in the Supplemental Material.

Seven DME profiles were measured for mixtures Nos. 8–14, representing seven effective temperatures. For each effective temperature, the A-factor of reaction R2 was adjusted to match the model prediction with the measured DME profile, resulting in an optimized reaction rate for the specific effective temperature. Seven rates were obtained and fitted to the Arrhenius expression to derive a new activation energy. The above process converged after two iterations. Figure 8 shows the measured k_{R2}, and the converged Arrhenius expression $k_{R2}/s^{-1} = 2.02 \times 10^{13} \exp(-34248\ K/T)$ over the temperature range of 994–1068 K at 30 bar. The uncertainty of the measured rate constant for R2 is also estimated to be ±30% because the four components of the uncertainty, *i.e.* the uncertainties in the effective temperature (±5.6 K, *i.e.* 25% in the measured rate), the mole fraction measurement (±15%), the effects from other reactions (±5%), and the fitting error (±5%), are similar to those in the measurement of k_{R1}. Details about the uncertainty identification and estimation were already introduced in Section 3.1. Sensitivity analysis was performed again based on the fitted k_{R2}, showing the production of DME is still dominated by R2 at 1080 K.

However, as shown in Fig. 8, discrepancies were found between the rates measured in this work and calculations from the literature [38–39]. Quantum chemistry calculations were performed in order to explore these discrepancies. We computed the potential profile of the two dominant DMC decomposition pathways with a high level quantum chemical method, *i.e.* CCSD(T)-F12/VTZ-F12//QCISD/cc-pVTZ, as shown in Fig. S6 in the Supplemental Material, along with the previous study by Peukert et al. [39] at the level of CCSD(T)/CBS//M062X/cc-pVTZ. The computed energy barriers for R2 from the two studies are almost identical. However, the computed frequencies at the level of M062X/cc-pVTZ have quite large deviations compared with the QCISD/cc-pVTZ frequencies, especially for low frequencies, as listed in Table S8 in the Supplemental Material. The QCISD method is suggested for studying such a transition state structure with resonance-stabilization characteristics. Among the temperature range of 994–1068 K, our RCM measurements agree very well with the calculated RRKM/ME rate constants in this work, but are lower than the data of Peukert et al. [39] by a factor of ~50. It is noted that Peukert et al. [39] measured the rate coefficients of DMC => $CH_3 + CH_3OC(O)O$ by ST and computed their values by the VariFlex code [58]. The phase space theory (PST) [59] was used to simulate the C–C bond fission with energies adjusted to fit their ST measurement for the C–C bond fission. The authors have stated that the simulated H concentration in their ST experiment was not sensitive to the rate constants of R2. Sun et al. [38] computed the DMC decomposition rate constants with the MESS code [55] by using the PES at CCSD(T)/CBS//M062X/cc-pVTZ and considering the conformational change between the *cis-trans* and *cis-cis* configurations. Their rate constants for R2 are also significantly lower than those of Peukert et al.'s [39] by a factor 10–20 over the temperate range of 900–1100 K at 10 atm. Considering the discrepancies between the computed k2 in this wok and those in Ref. [38], up to a factor of 4 over the temperature range of 900–1100 K, it can be mainly attributed to the entropy discrepancies between QCISD and M062X calculations since the energy barriers used in two studies are nearly the same.

4. Conclusions

A method was proposed to measure the rate constants in kinetically-simple systems using rapid compression machine (RCM) and fast sampling. The basic concept is that when the uncertainty of the concentration of a species is dominated by a single reaction, the rate of this reaction can be derived by measuring the concentration profile of this species. Considering the characteristic of RCM, the entire volume profile was used in the simulation to take into account the compression process and the heat loss effect.

As a validation of the proposed method, the rate of reaction CH_3OCHO (methyl formate, MF) => $CH_3OH + CO$ (R1) was determined by measuring the CO concentration in the MF pyroly-

sis in 948–1112 K, 30 bar, yielding the rate expression $k_{R1}/s^{-1} = 3.04 \times 10^{13} \exp(-30968\ K/T)$ with ±30% uncertainty. The excellent consistency of the measured rate constants with previous experimental [4] and theoretical [37] studies shows the merit of the proposed method. Then the rate constant of dimethyl carbonate (DMC) pyrolysis, DMC => CH_3OCH_3 (DME)+CO_2 (R2), was studied to demonstrate the utility of this method. Time resolved DME mole fraction was measured in DMC pyrolysis at 994–1068 K and 30 bar. The optimized rate expression is $k_{R2}/s^{-1} = 2.02 \times 10^{13} \exp(-34248\ K/T)$, which agrees well with the RRKM/Master Equation calculation based on a high level quantum chemical potential energy surface.

The method proposed herein can be used in various pyrolysis and oxidation systems as long as the uncertainty of the concentration of an individual species is predominantly influenced by a single reaction. Practically, some experimental design methods such as "sensitively entropy" [60] could be used to identify such systems. Considering that RCM has a longer characteristic time compared with that of ST, and GC can be used to quantify large molecules and multiple species simultaneously, the present method holds the potential to be a complementary tool for rate constant studies. Recognizing the limitations of the GC measurements, coupling RCM to fast-sampling time-of-flight mass spectrometer can be a useful tool for reaction rate measurements.

Acknowledgments

This work is supported by the National Natural Science Foundation of China (91541113, 91541112). The authors acknowledge helpful discussions with Can Huang and Tanjin He of Tsinghua University.

Supplementary materials

Supplementary material associated with this article can be found, in the online version, at doi:10.1016/j.combustflame.2017.05.006.

References

[1] F. Battin-Leclerc, J.M. Simmie, E. Blurock, Cleaner combustion, Springer, London, U.K. (2013), pp. 607–625.
[2] R.K. Hanson, D.F. Davidson, Recent advances in laser absorption and shock tube methods for studies of combustion chemistry, Prog. Energy Combust. Sci. 44 (2014) 103–114.
[3] R.K. Hanson, Applications of quantitative laser sensors to kinetics, propulsion and practical energy systems, Proc. Combust. Inst. 33 (2011) 1–40.
[4] W. Ren, K.Y. Lam, S.H. Pyun, A. Farooq, D.F. Davidson, R.K. Hanson, Shock tube/laser absorption studies of the decomposition of methyl formate, Proc. Combust. Inst. 34 (2013) 453–461.
[5] W. Ren, E. Dames, D. Hyland, D.F. Davidson, R.K. Hanson, Shock tube study of methanol, methyl formate pyrolysis: CH_3OH and CO time-history measurements, Combust. Flame 160 (2013) 2669–2679.
[6] H.S. Glick, W. Squire, A. Hertzberg, A new shock tube technique for the study of high temperature gas phase reactions, Symp. (Int.) Combust. 5 (1955) 393–402.
[7] R.S. Tranter, K. Brezinsky, D. Fulle, Design of a high-pressure single pulse shock tube for chemical kinetic investigations, Rev. Sci. Instrum. 72 (2001) 3046–3054.
[8] W. Tsang, Comparative rate measurements with single-pulse shock tube, J. Chem. Phys. 40 (1964) 1171–1172.
[9] W. Tsang, A. Lifshitz, Shock tube techniques in chemical kinetics, Annu. Rev. Phys. Chem. 41 (1990) 559–599.
[10] C.-J. Sung, H.J. Curran, Using rapid compression machines for chemical kinetics studies, Prog. Energy Combust. Sci. 44 (2014) 1–18.
[11] R.J. Tabaczynski, D.P. Hoult, J.C. Keck, High Reynolds number flow in a moving corner, J. Fluid Mech. 42 (1970) 249–255.
[12] S. Jakirlić, J. Volkert, H. Pascal, K. Hanjalić, C. Tropea, DNS, experimental and modelling study of axially compressed in-cylinder swirling flow, Int. J. Heat Fluid Flow 21 (2000) 627–639.
[13] D. Lee, S. Hochgreb, Rapid compression machines: heat transfer and suppression of corner vortex, Combust. Flame 114 (1998) 531–545.
[14] J. Würmel, J.M. Simmie, CFD studies of a twin-piston rapid compression machine, Combust. Flame 141 (2005) 417–430.
[15] G. Mittal, C.J. Sung, Aerodynamics inside a rapid compression machine, Combust. Flame 145 (2006) 160–180.
[16] G. Mittal, M.P. Raju, C.J. Sung, Computational fluid dynamics modeling of hydrogen ignition in a rapid compression machine, Combust. Flame 155 (2008) 417–428.
[17] G. Mittal, M.P. Raju, C.J. Sung, Vortex formation in a rapid compression machine: influence of physical and operating parameters, Fuel 94 (2012) 409–417.
[18] G. Mittal, C.J. Sung, A rapid compression machine for chemical kinetics studies at elevated pressures and temperatures, Combust. Sci. Technol. 179 (2007) 497–530.
[19] A.K. Das, M. Uddi, C.-J. Sung, Two-line thermometry and H_2O measurement for reactive mixtures in rapid compression machine near 7.6 µm, Combust. Flame 159 (2012) 3493–3501.
[20] M. Uddi, A.K. Das, C.-J. Sung, Temperature measurements in a rapid compression machine using mid-infrared H2O absorption spectroscopy near 7.6 µm, Appl. Opt. 51 (2012) 5464–5476.
[21] E.F. Nasir, A. Farooq, Time-resolved temperature measurements in a rapid compression machine using quantum cascade laser absorption in the intrapulse mode, Proc. Combust. Inst. 36 (2017) 4453–4460.
[22] D. Bradley, M. Lawes, M. Materego, Interpretation of auto-ignition delay times measured in different rapid compression machines, 25th International Colloquium on the Dynamics of Explosions and Reactive systems, 2015, 02-07 Aug, Leeds. http://eprints.whiterose.ac.uk/87762/.
[23] X. He, M.T. Donovan, B.T. Zigler, T.R. Palmer, S.M. Walton, M.S. Wooldridge, A. Atreya, An experimental and modeling study of iso-octane ignition delay times under homogeneous charge compression ignition conditions, Combust. Flame 142 (2005) 266–275.
[24] L.H.S. Roblee, A technique for sampling reaction intermediates in a rapid compression machine, Combust. Flame 5 (1961) 229–234.
[25] R. Minetti, M. Ribaucour, M. Carlier, C. Fittschen, L.R. Sochet, Experimental and modeling study of oxidation and autoignition of butane at high pressure, Combust. Flame 96 (1994) 201–211.
[26] M. Crochet, R. Minetti, M. Ribaucour, G. Vanhove, A detailed experimental study of n-propylcyclohexane autoignition in lean conditions, Combust. Flame 157 (2010) 2078–2085.
[27] G. Vanhove, Y. Yu, M.A. Boumehdi, O. Frottier, O. Herbinet, P.A. Glaude, F. Battin-Leclerc, Experimental study of tetrahydrofuran oxidation and ignition in low-temperature conditions, Energy Fuels 29 (2015) 6118–6125.
[28] D. Wilson, C. Allen, Application of a multi-zone model for the prediction of species concentrations in rapid compression machine experiments, Combust. Flame 171 (2016) 185–197.
[29] X. He, S.M. Walton, B.T. Zigler, M.S. Wooldridge, A. Atreya, Experimental investigation of the intermediates of isooctane during ignition, Int. J. Chem. Kinet. 39 (2007) 498–517.
[30] H.J. Curran, P. Gaffuri, W.J. Pitz, C.K. Westbrook, A comprehensive modeling study of iso-octane oxidation, Combust. Flame 129 (2002) 253–280.
[31] D.M.A. Karwat, S.W. Wagnon, M.S. Wooldridge, C.K. Westbrook, Low-temperature speciation and chemical kinetic studies of n-heptane, Combust. Flame 160 (2013) 2693–2706.
[32] D.M.A. Karwat, S.W. Wagnon, P.D. Teini, M.S. Wooldridge, On the chemical kinetics of n-butanol: ignition and speciation studies, J. Phys. Chem. A 115 (2011) 4909–4921.
[33] D.M.A. Karwat, S.W. Wagnon, M.S. Wooldridge, C.K. Westbrook, On the combustion chemistry of n-heptane and n-butanol blends, J. Phys. Chem. A 116 (2012) 12406–12421.
[34] S.M. Walton, D.M. Karwat, P.D. Teini, A.M. Gorny, M.S. Wooldridge, Speciation studies of methyl butanoate ignition, Fuel 90 (2011) 1796–1804.
[35] W. Ji, P. Zhang, T. He, Z. Wang, L. Tao, X. He, C.K. Law, Intermediate species measurement during iso-butanol auto-ignition, Combust. Flame 162 (2015) 3541–3553.
[36] S. Dooley, M.P. Burke, M. Chaos, Y. Stein, F.L. Dryer, V.P. Zhukov, O. Finch, J.M. Simmie, H.J. Curran, Methyl formate oxidation: speciation data, laminar burning velocities, ignition delay times, and a validated chemical kinetic model, Int. J. Chem. Kinet. 42 (2010) 527–549.
[37] D. Felsmann, H. Zhao, Q. Wang, I. Graf, T. Tan, X. Yang, E.A. Carter, Y. Ju, K. Kohse-Höinghaus, Contributions to improving small ester combustion chemistry: theory, model and experiments, Proc. Combust. Inst. 36 (2017) 543–551.
[38] W. Sun, B. Yang, N. Hansen, C.K. Westbrook, F. Zhang, G. Wang, K. Moshammer, C.K. Law, An experimental and kinetic modeling study on dimethyl carbonate (DMC) pyrolysis and combustion, Combust. Flame 164 (2016) 224–238.
[39] S.L. Peukert, R. Sivaramakrishnan, J.V. Michael, High temperature shock tube and theoretical studies on the thermal decomposition of dimethyl carbonate and its bimolecular reactions with H and D-atoms, J. Phys. Chem. A 117 (2013) 3718–3728.
[40] H. Di, X. He, P. Zhang, Z. Wang, M.S. Wooldridge, C.K. Law, C. Wang, S. Shuai, J. Wang, Effects of buffer gas composition on low temperature ignition of iso-octane and n-heptane, Combust. Flame 161 (2014) 2531–2538.
[41] P. Zhang, W. Ji, T. He, X. He, Z. Wang, B. Yang, C.K. Law, First-stage ignition delay in the negative temperature coefficient behavior: experiment and simulation, Combust. Flame 167 (2016) 14–23.
[42] D.G. Goodwin, H.K. Moffat, R.L. Speth. Cantera: An object-oriented software toolkit for chemical kinetics, thermodynamics, and transport processes, Version 2.2.1; 2016.
[43] R. Sivaramakrishnan, N.J. Labbe, W. Liu, M.J. Davis, A high temperature mechanism for methylformate combustion, 8th U.S. National Combustion Meeting, 2013 paper 070RK-0126.

[44] S.L. Peukert, R. Sivaramakrishnan, M.-C. Su, J.V. Michael, Experiment and theory on methylformate and methylacetate kinetics at high temperatures: Rate constants for H-atom abstraction and thermal decomposition, Combust. Flame 159 (2012) 2312–2323.
[45] S.L. Peukert, R. Sivaramakrishnan, M.C. Su, J.V. Michael, High temperature rate constants for H/D + methyl formate and methyl acetate, Proc. Combust. Inst. 34 (2013) 463–471.
[46] N.J. Labbe, R. Sivaramakrishnan, S.J. Klippenstein, The role of radical + fuel-radical well-skipping reactions in ethanol and methylformate low-pressure flames, Proc. Combust. Inst. 35 (2015) 447–455.
[47] J.A. Pople, M. Head-Gordon, K. Raghavachari, Quadratic configuration interaction. A general technique for determining electron correlation energies, J. Chem. Phys. 87 (1987) 5968–5975.
[48] T.H. Dunning, Gaussian basis sets for use in correlated molecular calculations. I. The atoms boron through neon and hydrogen, J. Chem. Phys. 90 (1989) 1007–1023.
[49] G. Knizia, T.B. Adler, H.-J. Werner, Simplified CCSD(T)-F12 methods: theory and benchmarks, J. Chem. Phys. 130 (2009) 054104.
[50] K.A. Peterson, T.B. Adler, H.-J. Werner, Systematically convergent basis sets for explicitly correlated wavefunctions: the atoms H, He, B–Ne, and Al–Ar, J. Chem. Phys. 128 (2008) 084102.
[51] A.D. Becke, A new mixing of Hartree-Fock and local density-functional theories, J. Chem. Phys. 98 (1993) 1372–1377.
[52] M.J. Frisch, G.W. Trucks, H.B. Schlegel, G.E. Scuseria, M.A. Robb, J.R. Cheeseman, G. Scalmani, V. Barone, B. Mennucci, G.A. Petersson, Gaussian 09, revision D. 01, Gaussian, Inc., Wallingford CT, 2009.
[53] H.J. Werner, P.J. Knowles, G. Knizia, F.R. Manby, M. Schütz, P. Celani, T. Korona, R. Lindh, A. Mitrushenkov, G. Rauhut, MOLPRO: A package of ab initio programs, University College Cardiff Consultants Ltd., Wales, UK, 2012.
[54] Y. Georgievskii, J.A. Miller, M.P. Burke, S.J. Klippenstein, Reformulation and solution of the master equation for multiple-well chemical reactions, J. Phys. Chem. A 117 (2013) 12146–12154.
[55] Y. Georgievskii, S.J. Klippenstein, 2016. MESS: Master equation system solver http://tcg.cse.anl.gov/papr/codes/mess.html.
[56] C. Eckart, The penetration of a potential barrier by electrons, Phys. Rev. 35 (1930) 1303–1309.
[57] R.G. Gilbert, S.C. Smith, Theory of unimolecular and recombination reactions, Blackwell Scientific Publication, Oxford London Edinburgh, 1990.
[58] S.J. Klippenstein, A.F. Wagner, R.C. Dunbar, D.M. Wardlaw, S.H. Robertson, J.A. Miller, VARIFLEX: VERSION 2.02 m, Argonne National Laboratory, Argonne, IL, 2010
[59] S.J. Klippenstein, J.I. Cline, Classical phase space theory for product state distributions with application to the v–j vector correlation, J. Chem. Phys. 103 (1995) 5451–5460.
[60] S. Li, T. Tao, J. Wang, B. Yang, C.K. Law, F. Qi, Using sensitivity entropy in experimental design for uncertainty minimization of combustion kinetic models, Proc. Combust. Inst. 36 (2017) 709–716.